Lipid Cubic Phases as Stable Nanochannel Network Structures for Protein Biochip Development: X-ray Diffraction Study

ARTICLE *in* LANGMUIR · JUNE 2003

Impact Factor: 4.46 · DOI: 10.1021/la0345284

4 AUTHORS, INCLUDING:

Angelina Angelova
Université Paris-Sud 11
88 PUBLICATIONS **1,679** CITATIONS
SEE PROFILE

Claudie Bourgaux
Université Paris-Sud 11
47 PUBLICATIONS **1,077** CITATIONS
SEE PROFILE

Lipid Cubic Phases as Stable Nanochannel Network Structures for Protein Biochip Development: X-ray Diffraction Study

Angelina Angelova,*,† Michel Ollivon,‡ Andrew Campitelli,† and Claudie Bourgaux‡,§

Biosensors group, IMEC, Kapeldreef 75, B-3001 Leuven, Belgium; UMR 8612 du CNRS, Equipe de Physico-Chimie des Systèmes Polyphasés, Centre d'Etudes Pharmaceutiques, 5 rue J. B. Clément, F-92296 Châtenay Malabry, France; and LURE, Université de Paris-Sud, F-91898 Orsay, France

Received March 27, 2003

Biocompatible nanochannel and mesoporous structures of a three-dimensional (3D) periodicity, facilitating protein entrapment at native conformations, constitute organized protective media of interest for the fast developing fields of protein biochips and affinity biosensors. Three-dimensional periodic nanochannel structures possessing reactive chemical groups, surface-exposed to the aqueous phase, are formed here in self-assembled mixtures of a nonlamellar lipid glycerylmonooleate (MO) and a maleimide(triethylene glycol)ether lipid (MTEG) under physiological hydration conditions and are investigated by high-resolution time-resolved synchrotron X-ray diffraction in the interval from 3 to 96 °C. The mechanism of formation and the structural parameters of two nonlamellar cubic phases Q^{224} and Q^{229} (of space groups *Pn*3*m* and *Im*3*m*) are monitored. The structural phase behavior of the MO/MTEG-based immunocubosome and proteocubosome mixtures, obtained upon incubation with immunoglobulin Fab fragments, whole IgG, albumin, transferrin, and fibrinogen at high concentrations, indicates that the cubic lattices exist in excess water as nanostructured channel networks. With the particular lipid composition of interest, the protein type only finely tunes these channel networks and they appear to be stable over a broad temperature interval. A new mechanism of protein entrapment within the 3D cubosome lipid networks is proposed.

Introduction

Capturing functional receptor molecules in surface-confined nano- and microstructures is an important task in protein biochip development for biosensor and proteomics applications.[1,2] Current physicochemical demands in biosensor design include enhancement of the bioanalytical sensitivity via nonlabeling approaches for signal amplification. Toward this aim, an increase of the sensor surface area for occurrence of affinity (ligand−receptor, antigen−antibody) binding might be a possible solution. This concept of biochip design involves interface evolution from a two-dimensional monolayer surface toward an infinite three-dimensional surface realized with biocompatible nanoporous composites or polymer films. Nanostructured materials of uniform pore distribution are significant also for the generation of nanocompartment chemical reactors, nanoporous membranes as functional catalytic surfaces or sensor elements, solid foams, porous materials of high-refractive index, nanostructured films for optics and laser technologies, nanorods and nanowire arrays for electronics applications, and superporous carriers for controlled peptide and protein drug delivery.

Supramolecular chemistry approaches[3,4] based on self-assembly of amphiphiles with reactive groups for biomolecular and surface binding have the capacity to generate smart functional materials with liquid-crystalline structures displaying large surface area. Thus, the existing lipid polymorphism[5,6] could be rationally explored in strategies to obtain nanostructured-capturing media for protein immobilization on sensor biochips. Bilayer-forming lipids have been intensively used in construction of biosensor systems with a ligand-gated ion channel switch,[7] affinity binding[8] and host−guest interactions.[9] On the other hand, lipids with a nonlamellar propensity, such as glyceryl monooleate (MO),[10,11] have turned up to be promising capturing materials in electrochemical biosensor design.[12] MO has been characterized on its own and in mixtures with fatty acids, surfactants, vitamins, and other biomolecules.[13−21] However, the most attractive

* To whom correspondence should be addressed. E-mail: Angelina.Angelova@imec.be.
† Biosensors group, IMEC.
‡ Centre d'Etudes Pharmaceutiques.
§ Université de Paris-Sud.

(1) Mitchell, P. *Nat. Biotechnol.* **2002**, *20*, 225−229.
(2) Mascini, M.; Minunni, M.; Guilbault, G. G.; Carter, R. In *Affinity Biosensors: Techniques and Protocols*; Rogers, K. R., Mulchandani, A., Eds.; Methods in Biotechnology, Vol. 7; Humana Press: Totowa, NJ, 1998; pp 55−76.
(3) Ikkala, O.; ten Brinke, G. *Science* **2002**, *295*, 2407−2409.
(4) Kato, T. *Science* **2002,** *295*, 2414−2418.
(5) Luzzati, V.; Spegt, P. A. *Nature* **1967**, *215*, 701−704.
(6) Luzzati, V.; Delacroix, H.; Gulik, A.; GulikKrzywicki, T.; Mariani, P.; Vargas, R. *Curr. Top. Membr.* **1997**, *44*, 3−24.
(7) Cornell, B. A.; Braach-Maksvytis, V. L. B.; King, L. G.; Osman, P. D. J.; Raguse, B.; Wieczorek, L.; Pace, R. J. *Nature* **1997**, *387*, 580−583.
(8) Bieri, C.; Ernst, O. P.; Heyse, S.; Hofmann, K. P.; Vogel, H. *Nat. Biotechnol.* **1999**, *17*, 1105−1108.
(9) Bayley, H.; Cremer, P. S. *Nature* **2001**, *413*, 226−230.
(10) Larsson, K. *Nature* **1983**, *304*, 664−664.
(11) Hyde, S. Y.; Andersson, S.; Ericsson, B.; Larsson, K. *Z. Kristallogr.* **1984**, *168*, 213-219.
(12) Razumas, V.; Kanapieniene, J.; Nylander, T.; Engstrom, S.; Larsson, K. *Anal. Chim. Acta* **1994**, *289*, 155−162.
(13) Lindblom, G.; Larsson, K.; Johansson, L.; Fontell, K.; Forsén, S. *J. Am. Chem. Soc.* **1979**, *101*, 5465−5470.
(14) Pisani, M.; Bernstorff, S.; Ferrero, C.; Mariani, P. *J. Phys. Chem. B* **2001**, *105*, 3109−3119.
(15) Takahashi, H.; Matsuo, A.; Hatta, I. *Mol. Cryst. Liq. Cryst.* **2000**, *347*, 231−238.
(16) Czeslik, C.; Winter, R.; Rapp, G.; Bartels, K. *Biophys. J.* **1995**, *68*, 1423−1429.
(17) (a) Caboi, F.; Amico, G. S.; Pitzalis, P.; Monduzzi, M.; Nylander, T.; Larsson, K. *Chem. Phys. Lipids* **2001**, *109*, 47−62. (b) Caboi, F.; Nylander, T.; Razumas, V.; Talaikyté, Z.; Monduzzi, M.; Larsson, K. *Langmuir* **1997**, *13*, 5476−5483.
(18) Aota-Nakano, Y.; Li, S. J.; Yamazaki, M. *Biochim. Biophys. Acta* **1999**, *1461*, 96−102.

10.1021/la0345284 CCC: $25.00
Published on Web 06/10/2003

scientific application of the MO cubic phase has been as a crystallization screen of membrane proteins,[22−25] but it has not been investigated toward human medical diagnostics applications. In addition to its bioadhesive features and particular rheology, the cubic phase of MO has the remarkable property that it may coexist with excess water in a wide temperature range (including body temperature).[11]

A bicontinuous cubic lattice may be considered as a nanoporous template (see Figure 5 bottom images P and D) involving an infinite lipid bilayer, which separates highly organized aqueous channel networks.[11,26] The 3D structures of bicontinuous inverted cubic lipid/water phases have been represented by infinite periodic minimal surfaces decorated by curved lipid bilayers and organized with particular 3D periodicities.[27−29] The cubic phases formed by amphiphilic molecules are soft and viscous, and they can finely swell or shrink at variance to the rigid, solid-phase materials of metal, oxide, or semiconductor nature (known to cause protein denaturation at surfaces).

An essential advantage of nonlamellar structures generated via spontaneous self-assembly upon lipid hydration is the very large surface area[30,31] as compared to that of monolayer and bilayer architectures. Cubic amphiphilic sponges have the capacity to capture and encapsulate both hydrophilic and hydrophobic molecules of various molecular sizes (from small molecules up to macromolecules such as proteins and polymers). It has been affirmed that proteins could be accommodated in lipid cubic phases either in the aqueous channel compartments (water-soluble proteins)[12,32−35] or in the lipid bilayer constituent (membrane proteins).[22−25] Generally, a protein would not denature in the protective soft lipid medium unless it is highly surface active and adsorbs at the interfaces with non-native conformations. Despite the great potential for utilization of nonlamellar lipid mixtures with entrapped proteins, previous structural studies of MO/protein/water phases[33,35] have mostly been performed with salt-free solutions and lipid concentrations around 50−60 wt %. Such experimental conditions can hardly ensure the full hydration of the protein and lipid components in a broad temperature interval and at aqueous salt compositions relevant to bioassays of current interest.

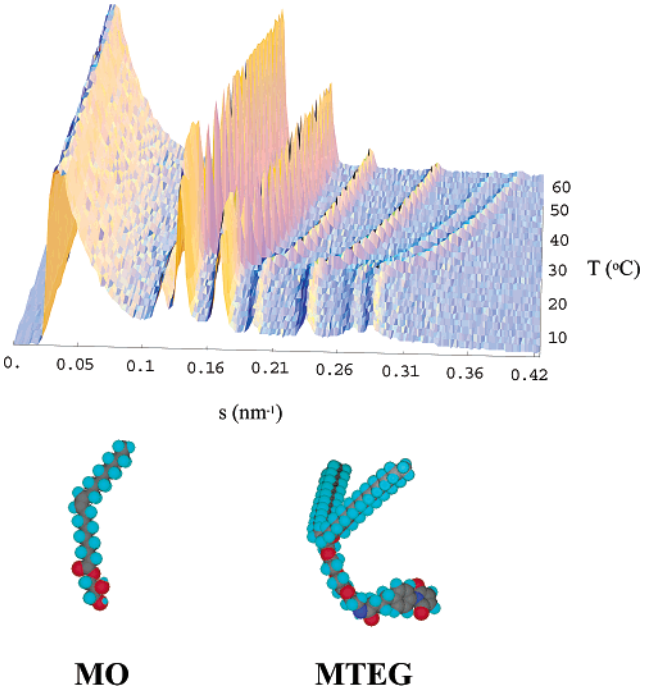

Figure 1. (top) Time-resolved synchrotron X-ray diffraction patterns of a fully hydrated MO/MTEG mixture (98/2 mol/mol) presented as reciprocal spacings s (nm^{-1}) vs temperature T (deg). The patterns are recorded at the scan rate 2 °C/min. Aqueous phase: 0.1 NaCl, 10^{-2} M phosphate buffer, pH 7. (bottom) Molecular models of the two uncharged amphiphiles monoolein and 1-{8-[4-(*p*-maleimidophenyl)butaroylamino]-3,6-dioxaloctyl}-2,3-distearyl glyceryl-DL-ether (MTEG).

The purpose of this study was to create and structurally characterize nonlamellar lipid/water phases for protein entrapments and immobilization on chips under physiological hydration conditions (excess water and appropriate salt concentration and pH). A lipid composition ensuring a nonlamellar propensity, a lack of surface charge, a triethylene glycol spacer in the lipid headgroup region, and chemical functionality introduced via reactive terminal groups was chosen for the structural study of protein immobilization in an organized 3D network medium. Monoolein was the main component of the nonlamellar lipid medium, and it was mixed with a second uncharged amphiphilic component, a maleimide(triethylene glycol)ether lipid (MTEG) (Figure 1), possessing a polar terminal group that is reactive to free SH groups. By means of time-resolved high-resolution synchrotron X-ray diffraction, we established that a small percent of this additive affects the cubic-to-lamellar phase transition temperature of pure MO and promotes the formation of stable and highly ordered nonlamellar structures in a salt environment of pH 7. Toward protein biochip and biosensor applications of the created 3D nanochannel networks in human blood analysis, we investigated also the influence of blood proteins on the structural phase behavior of the MO/MTEG mixtures. The lipid systems were incubated with selected proteins at concentrations in the range of those in human blood, and it was examined whether their 3D nonlamellar network organization will stably remain invariant of the blood protein type.

Experimental Section

Materials and Sample Preparation. The MTEG lipid 1-{8-[4-(p-maleimidophenyl)butaroylamino]-3,6-dioxaloctyl}-2,3-distearyl glyceryl-DL-ether (Northern Lipids Inc.) was mixed with 1-monooleoyl-*rac*-glycerol (Sigma) in chloroform (Merck, Uvasol) at desired molar ratios, and the solvent was evaporated under

(19) Borné, J.; Nylander, T.; Khan, A. *Langmuir* **2001**, *17*, 7742−7751.
(20) Angelov, B.; Ollivon, M.; Angelova, A. *Langmuir* **1999**, *15*, 8225−8234.
(21) Angelov, B.; Angelova, A.; Ollivon, M.; Bourgaux, C.; Campitelli, A. *J. Am. Chem. Soc.* **2003**, *125*, 7188−7189.
(22) Pebay-Peyroula, E.; Rummel, G.; Rosenbusch, J. P.; Landau, E. M. *Science* **1997**, *277*, 1676−1681.
(23) Kolbe, M.; Besir, H.; Essen, L. O.; Oesterhelt, D. *Science* **2000**, *288*, 1390−1396.
(24) de Kruijff, B. *Nature* **1997**, *386*, 129−130.
(25) Nollert, P.; Navarro, T.; Landau, E. M. *Method. Enzymol.* **2002**, *343*, 183−199.
(26) Scriven, L. E. *Nature* **1976**, *263*, 123−125.
(27) Funari, S. S.; Rapp, G. *Proc. Natl. Acad. Sci. U.S.A.* **1999**, *96*, 7756−7759.
(28) Schwarz, U. S.; Gompper, G. *Langmuir* **2001**, *17*, 2084−2096.
(29) (a) Garstecki, P.; Hołyst, R. *Langmuir* **2002**, *18*, 2529−2537. (b) Garstecki, P.; Hołyst, R. *Langmuir* **2002**, *18*, 2519−2528.
(30) For monoolein cubic lattice structures, this surface area has been referred to be around 400 m^2/g (ref 31).
(31) Jayne Lawrence, M. *Chem. Soc. Rev.* **1994**, *23*, 417−424.
(32) Mariani, P.; Luzzati, V.; Delacroix, H. *J. Mol. Biol.* **1988**, *204*, 165−188.
(33) Ericsson, B.; Larsson, K.; Fontell, K. *Biochim. Biophys. Acta* **1983**, *729*, 23−27.
(34) Razumas, V.; Larsson, K.; Miezis, Y.; Nylander, T. *J. Phys. Chem.* **1996**, *100*, 11766−11774.
(35) Leslie, S. B.; Puvvada, S.; Rathna, B. R.; Rudolph, A. S. *Biochim. Biophys. Acta* **1996**, *1285*, 246−254.

nitrogen flow during 4 h. The aqueous phase was prepared using 0.1 M NaCl in 10^{-2} M phosphate buffer (pH 7). Human transferrin (Sigma) and fibrinogen (Sigma) were dissolved in this buffer to the concentrations 3.6 and 4.0 mg/mL, respectively. Human chrompure immunoglobulin IgG (whole molecule) and Fab fragments (both FTIC-labeled and stabilized by bovine serum albumin) were received from Jacksson ImmunoResearch Inc. IgG and Fab solutions with concentration 4.0 mg/mL were prepared according to the instructions of the supplier in ultrapure water that was deoxygenated (these solutions contain 30 mg/mL bovine serum albumin as a stabilizer). Hydration, dispersion, and homogenization of the lipid/protein/water samples were done according to previously described procedures.[20,36] The samples, containing 30 wt % solid in the aqueous phase, were sealed in X-ray capillaries with the diameter 1.4 mm.

X-ray Diffraction. Synchrotron X-ray diffraction experiments were performed at beamline D24 of LURE (Orsay, France). The details of the experiments for investigating amphiphilic structural phase behavior were the same as those previously reported.[20] Temperature scans were effected at the scan rate 2 °C/min in the interval from 3 to 96 °C. The reciprocal X-ray spacings s were determined as $s = (2/\lambda) \sin \theta = 1/d = q/(2\pi)$ (where $\lambda = 1.489$ Å is the X-ray wavelength and 2θ is the scattering angle), and they were calibrated using tristearin ($d_{001} = 4.497$ nm) and silver behenate ($d_{001} = 5.8378$ nm) as standard samples. The lipid bilayer thickness, L, and the water channel thickness, D_w, in the generated 3D cubic lattice structures were determined using the model of Gartecki and Hołyst.[29]

Results and Discussion

Generation of Self-Assembled Lipid Cubic Phases of Biochip Relevance. Our synchrotron X-ray diffraction investigations established that pure MO fully hydrated in NaCl solution (phosphate buffer with pH 7) forms a lamellar phase in the interval from 0 to 19 °C. Therefore, protein biochip storage at low temperatures (around 4 °C), as well as protein bioassays requiring physiological salt and concentration conditions, could not utilize the nonlamellar phases of pure MO[11,16] because of their transformations into lamellar ones. In this study, we found that mixtures of MO and MTEG spontaneously form nonlamellar phases in a broad temperature range upon hydration in salt-containing excess buffer medium. On the other hand, the lipid MTEG shows a lamellar−lamellar phase transition in pure form at full hydration in buffer.[37]

Figure 1 shows time-resolved X-ray diffraction patterns of a MO/MTEG (98/2, mol/mol) mixture for the temperature interval from 4 to 60 °C. The obtained plots in the SAXS region are clearly distinguished from those of single-component MO in water and in NaCl solution, and they do not indicate phase separation of the lipids MO and MTEG into domains of individual components. (The same was found also with MO/MTEG mixtures at other molar ratios.)[37] Apparently, mixing of MO and MTEG leads to a new supramolecular organization characterized by a coexistence of two nonlamellar phases.

The long-range three-dimensional periodicity of the fully hydrated MO/MTEG (98/2 mol/mol) mixture is determined by two sets of X-ray peaks in the SAXS region. The peaks set with an onset at $s = 0.136$ nm^{-1} at 4 °C and s-values spaced in the ratio $\sqrt{2}$:$\sqrt{3}$:$\sqrt{4}$:$\sqrt{6}$:$\sqrt{8}$:$\sqrt{9}$:$\sqrt{10}$:$\sqrt{12}$:$\sqrt{14}$ were assigned to (110), (111), (200), (211), (220), (221), (310), (222), and (321) reflections of a cubic lattice Q^{224} ($Pn3m$ space group). The second peaks set was determined at an onset $s = 0.120$ nm^{-1} at 4 °C with peaks being spaced in the ratio $\sqrt{2}$:$\sqrt{4}$:$\sqrt{6}$:$\sqrt{8}$:$\sqrt{10}$:$\sqrt{12}$:$\sqrt{14}$:$\sqrt{16}$. The latter were assigned to (110), (200), (211), (220), (310), (222), (321), and (400) reflections of a cubic lattice Q^{229} (space group $Im3m$) (the two sets of X-ray peaks are displayed in Figures 3 and 6). The intensities of the reflections of the Q^{229} ($Im3m$) phase decrease upon heating above 24 °C and completely vanish above 42 °C. Because the peak intensities of this cubic structure are inferior to those of the Q^{224} phase, it follows that the volume fraction of the Q^{229} structure in the sample is minor at nonzero temperatures.

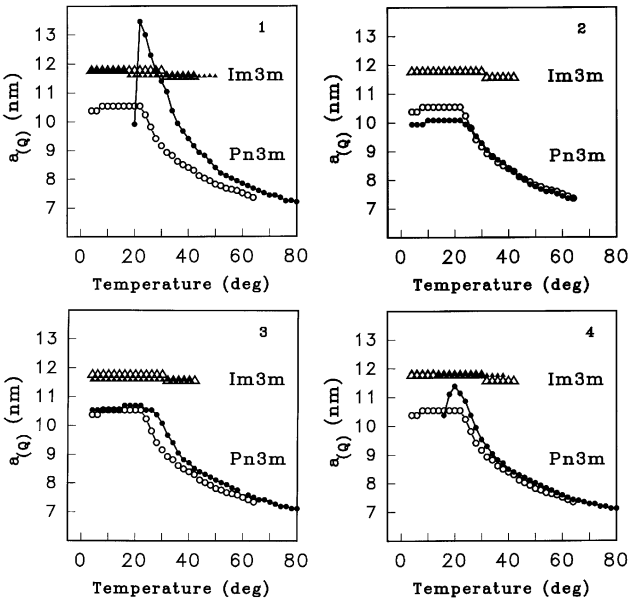

Figure 2. Temperature dependences of the lattice parameters, a(Q), of the cubic phases Q^{229} and Q^{224} formed by the MO/MTEG lipid mixture (98/2 mol/mol) at full hydration in 0.1 NaCl phosphate buffer solution with pH 7 (open triangles, $Im3m$ space group; open circles, $Pn3m$ space group). Frames 1−4 present the unit cell dimensions of the lipid cubic phases (filled triangles, $Im3m$ space group; filled circles, $Pn3m$ space group) determined upon incubation with protein solutions: 1, Fab fragment of immunoglobilin (stabilized with albumin); 2, human immunoglobulin (containing albumin as in 1); 3, human transferrin; 4, fibrinogen.

The lattice parameters of the two cubic phase structures in the MO/MTEG system, a(Q), were determined from the reciprocal slope of the linear plots s versus $(h^2 + k^2 + l^2)^{1/2}$, where (hkl) are the Miller plane indices. Figure 2 (open triangles) shows that the Q^{229} ($Im3m$) cubic structure is characterized by a unit cell dimension, $a(Q^{229}) = 11.77$ nm, that is nearly temperature invariant in the interval from 4 to 30 °C and is 11.57 nm in the interval from 32 to 42 °C. An essential temperature dependence of a(Q) was established with the Q^{224} ($Pn3m$) cubic structure at temperatures above 24 °C (Figure 2, open circles). Upon heating, $a(Q^{224})$ slightly increases from 10.38 nm (at 4 °C) to 10.54 nm (for 8 °C < T < 22 °C), followed by a continuous decrease from 10.23 nm (at 24 °C) to 7.51 nm (at 60 °C). At low temperatures below 22 °C, the coexisting Q^{224} and Q^{229} cubic lattices display close lattice parameters.

Lipid Cubic Phases Involving Sensor Protein Fragments and Human Blood Proteins. The proteins human immunoglobulin IgG (mixed with albumin), human transferrin, and fibrinogen were studied as major blood proteins in order to establish what structural influence they may exert on the supramolecular organizations of the MO/MTEG cubic phases when included in protein biochip assays. Nonlamellar phases were formed with MO/MTEG (98/2 mol/mol) systems with added monoclonal immunoglobulin Fab fragments or human blood proteins at concentrations required for bioassays without dilution. The Fab unit was investigated as a protein fragment with

(36) Angelova, A.; Ionov, R.; Koch, M. H. J.; Rapp, G. *Archives Biochem. Biophys.* **2000**, *378*, 93−106.
(37) Angelova, A.; et al. To be published.

sensor properties for detecting antibody−antigen recognition binding.

The time-resolved X-ray temperature scans performed with the lipid/protein/water systems demonstrated that cubic phase structures form with all water-soluble proteins which were investigated. Figure 2 (filled symbols, frames 1−4) presents a comparison between the lattice parameters, $a(Q^{224})$ and $a(Q^{229})$, of the MO/MTEG lipid cubic phases with incubated proteins and those determined in pure salt-buffer solution (open symbols). The effect of the proteins on the lattice parameter of the Q^{229} ($Im3m$) cubic phase is marginal, except for the IgG solution, for which the Q^{229} phase is not present at all at low temperatures. The values of $a(Q^{229})$ (filled triangles) are in the range between 11.90 and 11.57 nm (for 4 °C < T < 52 °C).

The lattice parameters of the Q^{224} ($Pn3m$) cubic phases formed upon addition of transferrin, IgG (mixed with albumin), and fibrinogen (Figure 2, filled circles, frames 2−4) do not differ notably at T > 25 °C from those of the lipid mixture hydrated in buffer (open circles). At variance, the dependence $a(Q^{224})$ versus temperature for the case of the Fab fragment (stabilized by albumin) is essentially shifted toward larger values with respect to those for the salt solution (Figure 2, frame 1). The obtained structural results indicate that the blood proteins do not destabilize the structural organization of the bicontinuous cubic media generated with lipid systems at room and higher temperatures, as they marginally influence the structural parameters of the created nanochannel networks. However, the phase behavior and lattice spacings of the complex lipid/protein/water phases are dependent on the protein type at low temperatures. An increase of the cubic unit cell dimension (Figure 2) corresponds to swelling of the nanoporous networks.

Mechanism of Formation of the Diamond-Type Nanochannel Networks in Fully Hydrated Lipid/Protein Phases. The inclusion of the sensor protein Fab fragment into the MO/MTEG/buffer mixture at full hydration leads to a rich thermal phase behavior of the binary lipid system (Figure 4, diagram 1), which allows us to analyze the mechanism of formation of the nanochannel networks in lipid/protein cubic phases and their structural transformations (Figure 3). We found that, at temperatures between 3 and 20 °C, a nonlamellar phase with a first peak centered at $s = 0.12$ nm^{-1} coexists with a lamellar bilayer phase. In the investigated SAX region, the bilayer phase displays a very strong first-order peak at $s = 0.202$ nm^{-1} and three higher-order diffraction peaks, which determine a lamellar spacing $d = 4.94$ nm. Peaks of the diamond Q^{224} ($Pn3m$) cubic phase begin to grow at T > 20 °C, and this is accompanied by vanishing of the lamellar bilayer peaks. Figure 3 shows the X-ray diffraction frames of the MO/MTEG/Fab/buffer system corresponding to the temperatures 22, 24, 26, 42, and 60 °C within the performed thermal scan (3−96 °C). The peaks analysis indicated a superposition of the reflections of the Q^{229} ($Im3m$) and Q^{224} ($Pn3m$) cubic phases in the range from 20 to 32 °C. If considered separately, the pattern at $T = 26$ °C could be attributed to a single diamond cubic lattice of the $Pn3m$ space group. However, the presence of the strong peak at $s = 0.12$ nm^{-1}, characteristic of the primitive Q^{229} ($Im3m$) lattice, both at T < 24 °C as well as at higher temperatures (up to 52 °C) implies that the X-ray pattern at $T = 26$ °C is resultant from coexisting Q^{229} and Q^{224} cubic structures. Owing to the peak overlapping of the two structures, one observes an increase of the peak intensity at $s = 0.12$ nm^{-1}.

The obtained structural results suggest that the diamond Q^{224} ($Pn3m$) cubic lattice network forms via thermally induced transformation from the lattice of the primitive Q^{229} ($Im3m$) cubic phase. At a particular temperature of the heating scan, the two nanochannel network structures are characterized by the same lattice parameters (namely $a(Q^{224}) = a(Q^{229}) = 11.77$ nm at T = 28 °C). The reflections of the two cubic phases become distinctly resolved in the interval from 34 to 52 °C, where the overlapping of the first-order diffraction peaks does not occur. Evidence is obtained here that the phase transition states during the formation and growth of the diamond cubic lattice are associated with an expanded unit cell dimension ($a(Q^{224}) = 13.0$ nm at 24 °C; Figure 2, frame 1) and an increased lipid bilayer thickness in this

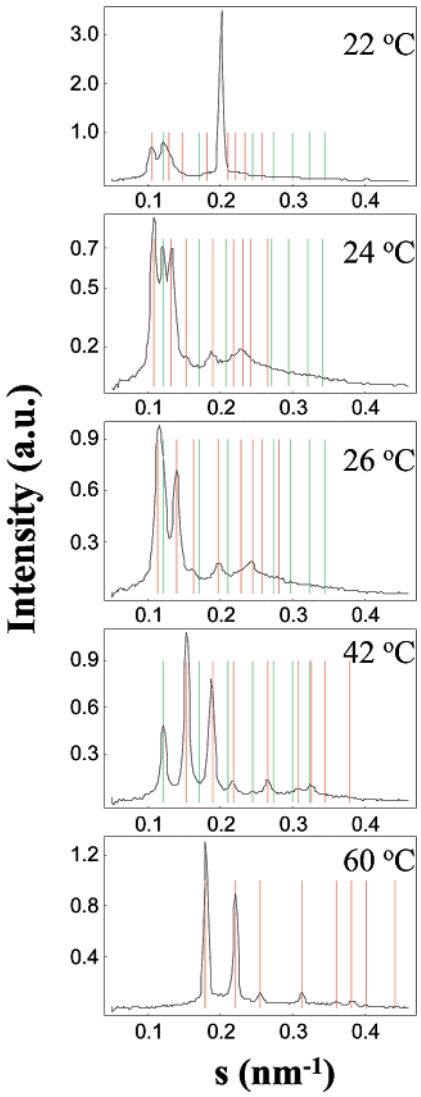

Figure 3. X-ray diffraction patterns of a MO/MTEG mixture (98/2 mol/mol) at full hydration in a solution of immunoglobulin Fab fragments (stabilized with albumin). The presented frames are acquired at the indicated temperatures from a heating scan performed at the rate 2 °C/min from 4 to 96 °C. The patterns are normalized, and the background is subtracted. From left to right, the red bars index the (110), (111), (200), (211), (220), (221), (310), and (222) reflections of a diamond cubic lattice Q^{224} ($Pn3m$) and the green bars consecutively denote the (110), (200), (211), (220), (310), (222), (321), and (400) reflections of a primitive cubic lattice Q^{229} ($Im3m$). The reflections of the diamond Q^{224} cubic phase arise from the overlapped reflections of the primitive Q^{229} cubic phase. A nonlinear regression peak fitting to eq 1 gave the following structural parameters for the diamond-type nanochannel network: (i) $T = 26$ °C, $a(Q^{224}) = 12.31$ nm, $L = 3.01$ nm, $D_w = 5.69$ nm; (ii) $T = 42$ °C, $a(Q^{224}) = 9.183$ nm, $L = 2.47$ nm, $D_w = 4.02$ nm; (iii) $T = 60$ °C, $a(Q^{224}) = 7.82$ nm, $L = 2.79$ nm, $D_w = 2.74$ nm.

swelled 3D network structure. We estimated using eq 1 that the diamond Q^{224} ($Pn3m$) cubic lattice network acquires, during its growth from the coexisting primitive Q^{229} ($Im3m$) cubic lattice, larger values of the lipid bilayer thickness, L, and the water channel thickness, D_w (L = 3.01 nm and D_w = 5.69 nm at T = 26 °C) in comparison to those determined for a single Q^{224} cubic phase formed on heating (L = 2.79 nm and D_w = 2.74 nm at T = 60 °C) (Figure 3).

Structural Phase Diagrams of Lipid/Protein/Water Phases Involving Sensor Protein Fragments and Human Blood Proteins. Figure 4 summarizes the phase sequences of the investigated amphiphilic mixtures determined from X-ray diffraction data on heating scans from 3 to 96 °C. The thermal phase behavior is characterized by several phases including lamellar (L), Q^{229} primitive cubic of the $Im3m$ space group (P), Q^{224} diamond cubic of the $Pn3m$ space group (D), inverted hexagonal HII (H), and inverted micellar (M).

The phase transition temperatures for the MO/MTEG/Fab/buffer system (Figure 4, diagram 1) are determined as follows:

$$Q^{229}(P) + L \overset{22\ °C}{\longleftrightarrow} Q^{229}(P) + Q^{224}(D) \overset{52\ °C}{\longleftrightarrow} Q^{224}(D) \overset{78\ °C}{\longleftrightarrow} Q^{224}(D) + H \overset{82\ °C}{\longleftrightarrow} H$$

Nonlamellar phases are present within the entire interval from 3 to 96 °C, and they are involved in particular phase coexistence regions. The L phase shows a temperature-invariant lamellar spacing (d = 4.94 nm) at 3 < T < 21 °C. An H_{II} phase is formed in the interval from 78 to 96 °C following the phase transformation of the diamond cubic phase. The inverted hexagonal lattice parameter varies from 5.54 nm (at 78 °C) to 5.34 nm (at 96 °C) upon increasing temperature.

For the MO/MTEG/IgG/buffer system (Figure 4, diagram 2), the diamond Q^{224} cubic phase appears to be a dominant nonlamellar structure at T < 60 °C:

$$Q^{224}(D) \overset{60\ °C}{\longleftrightarrow} Q^{224}(D) + H \overset{64\ °C}{\longleftrightarrow} H$$

At the investigated concentration, IgG exhibits a notable influence on the $Q^{229} \rightarrow Q^{224}$ phase transition temperature, suppressing the $Im3m$ cubic phase below 0 °C. The unit cell dimension of the H_{II} phase decreases upon heating from 5.71 nm (at 62 °C) to 5.15 nm (at 96 °C).

For the MO/MTEG/transferrin/buffer system (Figure 4, diagram 3), the Q^{224} phase is determined as the major cubic phase, while the peaks of the Q^{229} phase are essentially weaker but still detectable up to 40 °C):

$$Q^{229}(P) + Q^{224}(D) \overset{40\ °C}{\longleftrightarrow} Q^{224}(D) \overset{78\ °C}{\longleftrightarrow} Q^{224}(D) + H \overset{82\ °C}{\longleftrightarrow} H \overset{92\ °C}{\longleftrightarrow} M$$

The lattice parameter of the H_{II} phase changes from 5.54 nm (at 78 °C) to 5.43 nm (at 90 °C). The M phase displays a single isotropic peak centered at $s \sim 0.23$ nm^{-1}.

The temperature-induced experimental phase sequence for the MO/MTEG/fibrinogen/buffer system (Figure 4, diagram 4) is

$$L + Q^{229}(P) \overset{20\ °C}{\longleftrightarrow} Q^{229}(P) + Q^{224}(D) \overset{40\ °C}{\longleftrightarrow} Q^{224}(D) \overset{76\ °C}{\longleftrightarrow} Q^{224}(D) + M \overset{82\ °C}{\longleftrightarrow} M$$

The intensities of the lamellar phase reflections decrease at T > 16 °C, and the L spacing d = 4.94 nm is temperature insensitive. The diamond (D) cubic phase grows from the primitive (P) one in the temperature range from 18 to 24 °C, and its reflections are very intensive and clearly resolved at T > 26 °C. The isotropic M phase is detected with a peak maximum at s = 0.22 nm^{-1}.

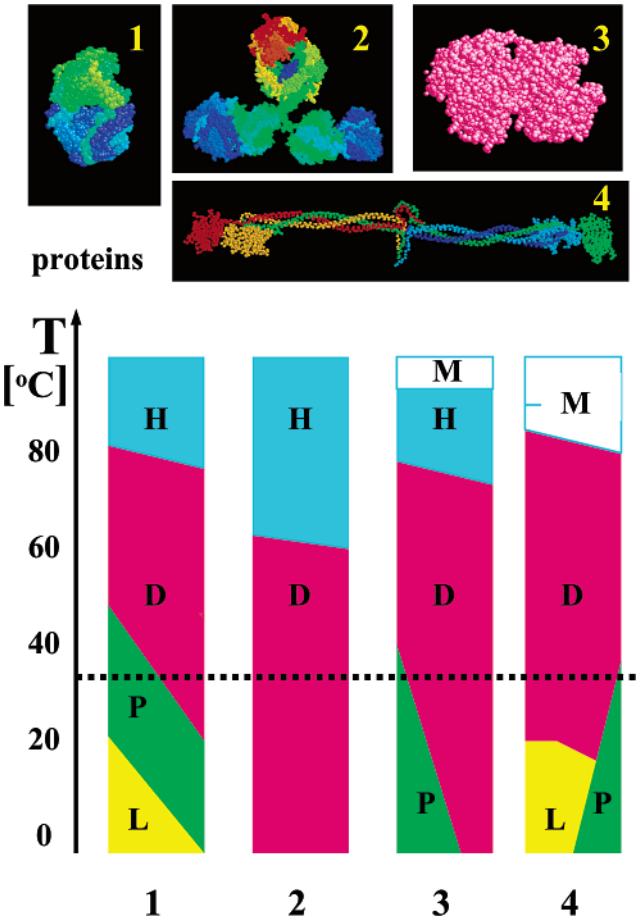

Figure 4. Diagram of the temperatute-induced phase sequences of MO/MTEG mixtures (98/2 mol/mol) involving proteins (1−4) at full hydration. The structures are determined from time-resolved X-ray diffraction patterns during heating scans. Notation: L, lamellar; P, Q^{229} primitive cubic ($Im3m$ space group); D, Q^{224} diamond cubic ($Pn3m$ space group); H, inverted hexagonal (H_{II}); M, inverted micellar phases. The dashed line indicates the body temperature. The images show (not to scale) the protein molecular shapes: 1, Fab fragment of IgG1 (MW ~ 48 kDa); 2, immunoglobulin (MW ~ 145 kDa); 3, transferrin (MW ~ 75 kDa); 4, fibrinogen (MW ~ 340 kDa).

The nanochannel network structures constituting the nonlamellar cubic phases formed by the MO/MTEG/protein/water systems appear to be highly stable, as evidenced by the presented thermal phase behavior. The MTEG lipid induces at 0 < T < 40 °C the formation of a Q^{229} ($Im3m$) phase, which has a larger water content[38] in comparison to that of the pure MO cubic phase ($Pn3m$). Both the diamond (D) and the primitive (P) cubic lattices are water-permeable, and the $Im3m$ lattice turned up to be temperature invariable.

General Phase Diagram: Influence of Water Concentration and Temperature. Structural investigations of self-assembled amphiphilic phases, performed at constant temperature under conditions of limited water in the systems, have deduced the following sequence of cubic−cubic phase transitions with increasing water content:[38]

Q^{230}(gyroid G, $Ia3d$) →
Q^{224}(diamond D, $Pn3m$) → Q^{229}(primitive P, $Im3m$)

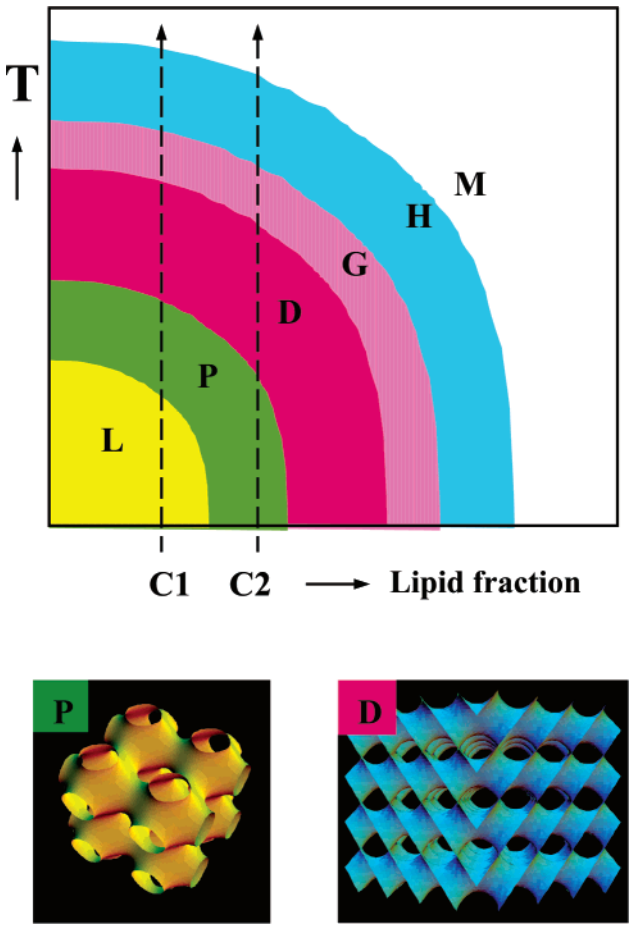

Figure 5. (top) Schematic structural phase diagram (temperature vs lipid weight fraction) indicating the possible lamellar-to-nonlamellar sequences for lipid/protein mixtures at full hydration. Notation: L, lamellar; P, Q^{229} primitive cubic ($Im3m$ space group); D, Q^{224} diamond cubic ($Pn3m$ space group); G, Q^{230}, gyroid ($Ia3d$ space group); H, inverted hexagonal (HII); M, inverted micellar phases. Different chemical compositions (C1, C2, ...) lead to various (L, P, D, G, H, M) phases upon heating. (bottom) 3D presentations of the structure of the nanochannel networks in Q^{229} ($Im3m$) and Q^{224} ($Pn3m$) cubic phases obtained with primitive (P) and diamond (D) type infinite periodic minimal surfaces (images created from simulations in ref 42).

In fact, the Q^{230} cubic phase has been experimentally established in lipid/protein mixtures in lack of excess water.[33,35]

Under excess water conditions (full hydration), the general phase sequence following from theoretical predictions[28] includes various lamellar and nonlamellar phases (Figure 5), which may be induced upon increasing of temperature or decreasing of pressure:

lamellar (L) →
Q^{229}(primitive, P) → Q^{224}(diamond, D) →
Q^{230}(gyroid, G) → inverted hexagonal (H) →
inverted micellar (M)

Figure 5 demonstrates that an increase in temperature could lead to diverse phase sequences of amphiphilic systems characterized by different chemical compositions. Depending on the chemical composition (e.g. C1, C2, or other), some of the above phases may not be experimentally detected.

The results obtained in this study at full hydration (Figure 4) reveal that adding of protein components to the MO/MTEG/water system has an analogous effect on the lipid phase sequence as the increasing or decreasing of temperature. Incubation with immunoglobulin causes a shift of the primitive-to-diamond cubic−cubic transition to temperatures below 0 °C, thus favoring the formation of a single cubic Q^{224} phase at low temperatures (Figure 4, diagram 2). The addition of transferrin to the hydration medium (Figure 4, diagram 3) does not alter the $Q^{229} \rightarrow Q^{224}$ phase transition temperature of the original lipid mixture. Incubating in buffer solutions of Fab fragments (Figure 4, diagram 1) or fibrinogen (Figure 4, diagram 4) shifts the lamellar-to-nonlamellar lipid phase transition to temperatures above 0 °C, which results in the stabilization of the diamond cubic Q^{224} lattice network up to very high temperatures (>80 °C). Figure 4 shows that all protein-containing systems are characterized by cubic P and/or D type structures at room and body temperatures. A gyroid Q^{230} ($Ia3d$) cubic phase was not observed with the investigated lipid/protein/buffer compositions, at variance to the studies performed with limited water amounts in amphiphilic systems.[32,35]

The self-assembly supramolecular structures are rationally related with the molecular geometry of the amphiphiles in the theory of Israelachvili.[39] The latter treats the resulting structure type in terms of a critical packing parameter $\eta = V_{hc}/(h_{hc}A)$, where A is the cross-sectional area of the hydrophilic headgroups at the headgroup/water interfaces of the amphiphilic assembly, and V_{hc} and h_{hc} are the volume and the extended-state length of the hydrophobic chains of the molecule. For nonlamellar phases $\eta > 1$ (namely $\eta = 1.06$ for a primitive Q^{229} ($Im3m$) cubic structure, $\eta = 1.08$ for a diamond Q^{224} ($Pn3m$) cubic lattice, and $\eta = 1.1$ for an inverted hexagonal phase H_{II} phase), while η is equal to or less than unity for a lamellar phase ($0.5 < \eta < 1$). Changes in the amphiphile's geometry, which are reflected in changes in *Vhc* and *hhc* or *A*, affect the type of the self-assembled supramolecular structure.[20,21,36,38,40,41] If the packing factor η decreases, the interfacial monolayer curvature decreases, and the supramolecular structure transforms into a lamellar or a micellar one.

MO is a nonlamellar lipid with $\eta = 1.07$,[20] and it spontaneously forms a cubic phase upon hydration in excess deionized water. The shift of the lamellar-to-cubic phase transition temperature of pure MO hydrated in salt environment to a nonzero value, 19 °C (established here for 0.1 NaCl M buffer solution with pH 7), corresponds to a decrease in the MO molecular packing parameter ($\eta \sim 1.0$). This could be explained by modifications in the lipid headgroup hydration shell and, respectively, in the effective interfacial area per amphiphilic molecule, *A*, as a result of salt influence. On the other hand, nonlamellar phases are favorably formed upon the hydration of the binary MO/MTEG mixtures in salt buffer solutions. Evidently, the large hydrophobic volume of the double-chained lipid MTEG (Figure 1) contributes to an increase of the average η in the system, and one establishes a spontaneous cubic phase formation ($\eta > 1$). The created nonlamellar structures are probably stabilized also by the tri(ethylene glycol) moieties in the headgroups of the lipid bilayers, which may exert steric repulsion in the aqueous compartments.

(38) Seddon, J. M. *Biochem. Biophys. Acta* **1990**, *1031*, 1−69.
(39) Israelachvili, J. N. *Intermolecular and Surface Forces*; Academic Press: New York, 1992; pp 380−382.
(40) Keller, S. L.; Gruner, S. M.; Gawrisch, K. *Biochim. Biophys. Acta* **1996**, *1278*, 241−246.
(41) Meunier, J., Langevin, D., Boccara, N., Eds. *Physics of Amphiphilic Layers*; Springer-Verlag: 1987.
(42) Angelov, B. *Mod. Phys. Lett. B* **2002**, *16*, 225−230.

Included proteins and peptides particularly influence the nonlamellar lipid phase behavior. Moreover, the structural effects are concentration dependent.[36] Peptides such as alamethicin, gramicidin, and melittin have been shown to promote the formation of cubic phases in lipid systems displaying lamellar-liquid-crystalline (Lα)-to-inverted hexagonal (H_{II}) phase transitions.[36,40] These peptides are surface active, incorporate into the headgroup region of the membranes, and change the monolayer curvature properties of the lipid bilayers. The spontaneous self-assembly of cubic phases,[36,40] resulting from the induction of curved structure formation, is associated with a suppression of the lamellar-to-nonlamellar phase transition temperature to a value below 0 °C. For such systems, the cubic phase stabilization results from the accommodation of peptide molecules from the aqueous phase into the polar lipid headgroup regions and direct influence on the lipid packing and mean monolayer curvature. Other proteins, such as cytochrome *c*, have shown a destabilizing effect on the cubic phase formation of the nonlamellar lipid monoolein, as judged from the significant decrease of the cubic-to-inverted hexagonal (H_{II}) phase transition temperature.[34] This has been attributed to interaction of the protein with the MO bilayer.

It should be stressed that proteins as well as other molecules, considered as solutes with kosmotropic or chaotropic properties, in the aqueous phase of the amphiphilic system may exert an integral hydration effect on the lipids. Moreover, highly hydrated proteins will compete with the lipid headgroups for hydration water. The influence on the hydration shell of the lipid headgroups will be associated with expansion or condensation of the effective interfacial area per amphiphilic molecule, *A*, and could induce protein concentration-dependent lipid phase transformations. It could be supposed that Fab fragments with high solution concentration (4 mg/mL) cause an increase in the effective area per lipid molecule in the MO/MTEG system and a decrease in the mean packing parameter, which shifts the phase sequence toward lamellar phase formation (Figure 4, diagram 1). This effect was established to be concentration dependent. We found that when the protein concentration is reduced four times, a lamellar phase does not appear at $T > 0$ °C in the phase sequence, and the MO/MTEG/Fab/buffer sample is entirely characterized by a cubic phase organization (data not shown here), as that of the original lipid mixture in buffer.

Protein Entrapment with Nanostructured 3D Lipid Networks. The labyrinthine structures of the lipid cubic phases include 3D networks of aqueous tubes (Figure 5, bottom images) that are separated by a continuous bilayer of lipid molecules.[6] The periodic supramolecular organization is subdivided into distinct polar regions branched out by a hydrocarbon continuum. The aqueous channels are not strictly cylindrical; they display ovaloid cross sections viewed at individual planes of the cubic lattice (Figure 5, bottom images P and D). Theoretical simulations of the scattering patterns of cubic phases have revealed that the relative intensities of the diffraction peaks for a given chemical composition depend on the thickness of the lipid bilayer, determining the distribution of the electron density in the 3D system. The thickness of the lipid bilayer in cubic lipid phases has been explicitly theoretically derived for the first time by Gartecki and Hołyst.[29] According to their recent model, the lipid bilayer thickness, *L*, in a cubic lipid phase can be estimated from the structural lattice parameter, *a*, on the basis of eq 1. The latter relates the intensities in the experimental X-ray

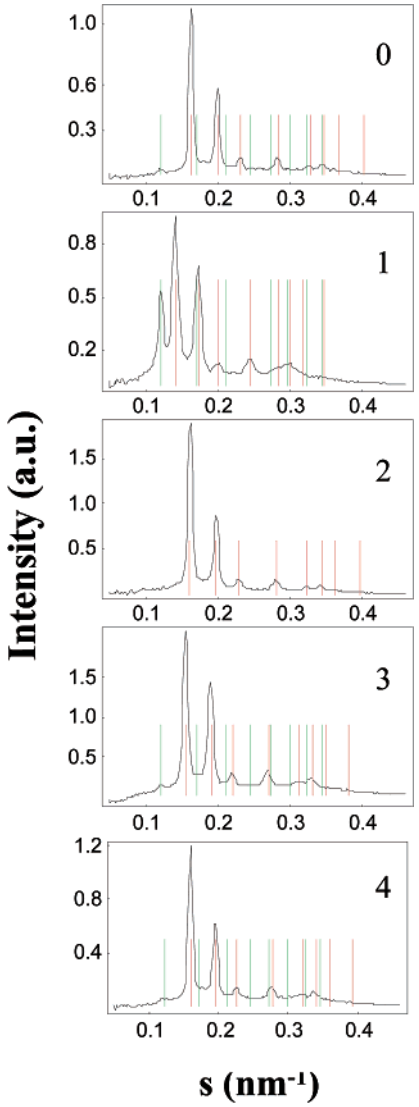

Figure 6. X-ray diffraction patterns of a MO/MTEG mixture (98/2 mol/mol) at full hydration in solutions of (0) 0.1 M NaCl, phosphate buffer pH 7; (1) immunoglobulin Fab fragments (stabilized with albumin); (2) human IgG (stabilized with albumin); (3) human transferrin; and (4) fibrinogen. The patterns correspond to body temperature, and they are extracted from heating scans recorded at the rate 2 °C/min. Toward peaks fitting, the patterns are normalized and the background is subtracted. The red bars denote, from left to right, the (110), (111), (200), (211), (220), (221), (310), and (222) reflections of a diamond cubic lattice Q^{224} ($Pn3m$), and the green bars consecutively index the (110), (200), (211), (220), (310), (222), (321), and (400) reflections of a primitive cubic lattice Q^{229} ($Im3m$). The results for *L* and D_w are given in Table 1.

patterns with model scattering intensities defined as

$$I_{hkl}^{(\mathrm{mod})}(\mathrm{L}) = M_{hkl}\left[F_{hkl}^{S*}\frac{\sin(\alpha_{hkl}\pi(h^2+k^2+l^2)^{1/2}L^*)}{\alpha_{hkl}\pi(h^2+k^2+l^2)^{1/2}}\right]^2 \quad (1)$$

where $L^* = L/a$ is the dimensionless lipid layer thickness, F^{S*} is the dimensionless structure factor, M_{hkl} is a multiplicity factor, and α_{hkl} are correction parameters for particular cubic lattice types.[29] For our systems, the values of *a* are given in Figure 2.

Figure 6 shows normalized X-ray diffraction patterns of MO/MTEG protein-free and protein-containing lipid cubic phases at body temperature (37 °C). To estimate the lipid bilayer thickness, *L*, and the water channel thickness,

Table 1. Cubic Lattice Parameters $a(Q^{229})$ and $a(Q^{224})$ of Primitive Q^{229} ($Im3m$) and Diamond Q^{224} ($Pn3m$) Cubic Structures Determined at Body Temperature (37 °C) for MO/MTEG Mixtures (98/2 mol/mol) Hydrated in Excess Buffer Solution (Figure 6, 0) and upon Incubation with Proteins (Figure 6, 1−4)[a]

	none	Fab	IgG	transferrin	fibrinogen
$a(Q^{229})$ (nm)	11.57	11.688		11.57	11.57
$a(Q^{224})$ (nm)	8.66	9.988	8.74	9.095	8.90
L (nm)	3.18	2.836	3.20	3.34	3.29
D_w (nm)	2.95	4.22	2.98	3.09	3.0
M (Da/mol)		48 000	145 000	75 000	340 000
protein structure file PDB		1ACY	1IGT	1JNF	1DEQ
protein extended molecular dimensions (nm^3)		7.7 × 5.2 × 4.1	16.1 × 12.3 × 6.6	8.8 × 6.5 × 4.5	44.2 × 5.1 × 6.0

[a] The lipid bilayer thickness, L, and the water channel thickness, D_w, for the Q^{224} phase are estimated via nonlinear fitting of the experimental patterns in Figure 6 to eq 1. The dimensions of the protein molecules are determined from PDB sources,[43−46] and M denotes the protein molecular weight.

D_w, characterizing the investigated 3D channel networks, the background of the patterns was subtracted and nonlinear regression fits were performed (with $r^2 > 0.99$) using eq 1. For a diamond cubic lattice, $D_w = 0.707a - L$. The results for L (ranging from 2.8 to 3.3 nm) and D_w (in the range from 2.9 to 4.2 nm) at $T = 37$ °C are presented in Table 1. The presence of immunoglobulin (mixed with albumin), transferrin, and fibrinogen does not essentially modify the lipid bilayer thickness and the aqueous channel sizes as compared to those in a protein-free system.

Previous investigations of cubic phases[32,33] have assumed that water-soluble proteins are accommodated in the water channels of the bicontinuous cubic lattices. On the basis of new structural information, the present investigation can hardly support the hypothesis that protein macromolecules are placed within the aqueous channels of the diamond-type ($Pn3m$) bicontinuous cubic lattice. It also questions whether even small proteins could be freely located inside the water nanochannels, which appear to have a diameter around 3−4 nm both in pure MO and in the MO/MTEG systems (this dimension corresponds to the aqueous core of the channels and does not include the lipid bilayer thickness). Thus, a geometrical consideration of the peptide leptin, which has a molecular weight (MW) of only 16 kDa, reveals that the extended-state molecular dimensions of this rather small protein ($4.4 \times 3.2 \times 3.1$ nm^3) may exceed the internal pore diameter in the diamond-type nanochannel networks. Hence, it is irrational to suppose that the medium- (MW 48 kDa) and large-size (MW 145−340 kDa) proteins, considered in this study (molecular dimensions presented in Table 1), would be regularly located within the nanopores of the created 3D network structures. However, these proteins appear to be confined within the cubic phase networks, as they remain in the systems after three times washing with buffer solution and overnight dialysis against pure buffer. Despite the fact that the proteins are too large to be accommodated inside the nanopores, they do not separate into macroscopic micellar aggregates easily detectable in the excess water environment of the cubic phase. On the other hand, the protein presence in the lipid cubic phase is easily detectable by spectroscopic measurements.[37]

Therefore, a new mechanism of protein entrapment within the 3D nanostructured cubic lipid media could be proposed on the basis of the presently available structural information. We consider the bicontinuous cubic phase medium as a nanostructured assembly of cubosome particles displaying 3D cubic lattice periodicity. Proteins likely locate at the interfaces between the cubosome nanoparticles in the system or associate to the surface of the interconnected cubosomal entities, owing to their surface activity and intermolecular interactions. As the understanding of the mechanism of entrapment of water-soluble proteins into lipid cubic phases is presently limited, complementary experimental methods are presently involved toward the verification of this new concept.

In this study, we demonstrated additional capacities of the synchrotron X-ray diffraction method to investigate lipid/protein/water systems, that exceed the determination of the peak positions and lattice spacings of cubic lipid phases. Time-resolved X-ray diffraction scans in the SAXS region allowed us also to monitor temperature-induced cubosome-to-homogeneous texture reorganization of the complex samples as well as to determine the thickness of the lipid bilayers and the water channels of the network cubic structures on the basis of a recent theoretical model.[29] Domain organization of the samples involving nano- and microaggregates, such as cubosomes or micellar particles, results in a superimposed broad micellar-like background[21] in the X-ray patterns centered around $s = 0.22-0.25$ nm^{-1}. Heating, which promotes the mixing of the components in the samples, leads to X-ray patterns that are indicative of a macroscopically homogeneous mesophase formation.

Conclusion

Nanostructured lipid/protein cubosome materials were obtained here by thermodynamic self-assembly, and they were shown to stably exist under excess water conditions and physiological temperatures. The created structures are highly ordered and possess uniform pores over a large scale. Such smart biomaterials with nanochannel network architecture provide a protective medium for surface immobilization of biomolecules and encapsulation of proteins. The introduced chemical functionality is useful for grafting of the cubosome assemblies on solid substrates toward further investigations for biochip and biosensor applications. The nanochannel networks formed in the cubic lipid phases turned up to be stable in a broad temperature range and can be utilized in blood analysis, as they are not disrupted by medium- and large-size proteins. Applications of the created nanostructured systems are anticipated in protein biochip development, diagnostics, and therapeutics, as well as in synthesis of nanowires and nanorods via emulsifier templates.

Acknowledgment. This work was supported by the EC through LURE project BD 015-01. A.A. thanks B. Angelov for mathematical algorithms allowing rational synchrotron X-ray data analysis.

LA0345284

(43) Ghiara, J. B.; Stura, E. A.; Stanfield, R. L.; Profy, A. T.; Wilson, I. A. *Science* **1994**, *264*, 82−85.
(44) Harris, L. J.; Larson, S. B.; Hasel, K. W.; McPherson, A. *Biochemistry* **1997**, *36*, 1581−1597.
(45) Hall, D. R.; Hadden, J. M.; Leonard, G. A.; Bailey, S.; Neu, M.; Winn, M.; Lindley, P. F. *Acta Crystallogr., Sect. D* **2002**, *58*, 70−80.
(46) Brown, J. H.; Volkmann, N.; Jun, G.; Henschen-Edman, A. H.; Cohen, C. *Proc. Natl. Acad. Sci. U.S.A.* **2000**, *97*, 85−90.